Cement & Concrete Composites 37 (2013) 30–36

Contents lists available at SciVerse ScienceDirect

Cement & Concrete Composites

journal homepage: www.elsevier.com/locate/cemconcomp

Influence of the pore network on hydrogen diffusion through blended cement pastes

Cédric Boher [a,b], Fabien Frizon [b], Sylvie Lorente [a,*], Florence Bart [b]

[a] Université de Toulouse, UPS, INSA, LMDC (Laboratoire Matériaux et Durabilité des Constructions), 135 Avenue de Rangueil, F-31077 Toulouse Cedex 04, France
[b] CEA, DEN, DTCD/SPDE/LP2C – Marcoule, F-30207 Bagnols-sur-Cèze, France

ARTICLE INFO

Article history:
Received 14 February 2012
Received in revised form 12 December 2012
Accepted 15 December 2012
Available online 23 December 2012

Keywords:
Gas diffusion
Cement paste
Virtual pore network
Water saturation

ABSTRACT

This article presents a study on the influence of the pore size distribution on gas diffusion through CEM V cement pastes, for different water saturation degrees. The numerical results are compared to the experimental hydrogen diffusion coefficients obtained with water saturation levels ranging from 20% to 95%. The model developed in our research group accounts for the various types of transfer through the pore network: Knudsen diffusion or molecular diffusion depending on the pore size, together with hydrogen diffusion through water. The virtual pore network is created from mercury porosimetry data as a result of the combination of different sizes pore families. By testing different combinations, we could propose pore arrangements leading to diffusion coefficients corresponding to the experimental ones, and show how the combinations of the biggest pore family contribute to control the gas diffusion process.

1. Introduction

Most of low or intermediate level radioactive wastes packages are either based on a cement-based matrix or stored into concrete containers. The radiolysis of interstitial water or of organic materials, or other processes such as corrosion, may produce explosives gas, among which hydrogen. The French National Agency for Radioactive Waste Management (ANDRA) specifies that hydrogen concentration must be lower than 2% in wastes packages. Experimental investigations were recently presented on small scale and real scale samples to measure the diffusion coefficients of cementitious materials [1,2]. The results highlighted the impact of environmental conditions such as the moisture level on the diffusive properties [3–6]. Yet, a diffusion coefficient is a macroscopic parameter that does not reveal the impact of the pore size distribution on the gas transfer. Indeed, the modes of transport of hydrogen under a concentration difference depend on the pores size: the hydrogen transfer may be due to free (or Knudsen) diffusion, or to molecular diffusion. Hydrogen diffusion through cement pastes is mainly influenced by (i) the pores size of the material which depends on its formulation (cement type, water/cement ratio), and (ii) the water saturation degree which depends on the storage conditions (relative humidity). The objective of this paper is to study how the diffusion coefficient of hydrogen through cement pastes evolves as a function of the controlling parameters listed above.

2. Materials and experiments

The investigated materials were CEM V/A (Calcia, Airvault) cement pastes, i.e. ordinary Portland cement with addition of fly ashes and slag [7]. The water/cement ratios (W/C), were 0.35, 0.4, 0.45 and 0.50. This ratio was the unique formulation parameter. The samples were kept in a room at controlled temperature (20 °C) and relative humidity (95%) for 24 h after casting. Then followed an endogenous curing period of 3 years in a room at 20 °C.

Due to the amount of formed hydrates, the W/C ratio has impact on the pore size distribution as described by the mercury intrusion porosimetry results presented in Fig. 1 and the water porosity values given in Table 1 [8]. Fig. 1 documents the contribution of the capillary porosity to the overall porosity in the case of the highest W/C ratios. According to the figure, the ratio between the volume of the pores from the gel (1.5–10 nm) to the capillary pores (70 nm to 2 μm) is about 4 when W/C = 0.35. This ratio is about 3 for W/C = 0.50. The meso-pore size (radius around 30 nm) does not seem to be affected by the change in W/C ratio.

The cement pastes were cast into cylindrical molds of 11 cm in diameter and 6 cm in height. After curing for 3 months, 3 cylinders of 4 cm in diameter were drilled from the 11 cm diameter original cylinder, and cut into 2 cm thick samples before storage. Note that the ends of the cylinders were not kept for the experiments. The samples were distributed into sealed boxes, maintained at 20 °C. The Relative Humidity (RH) in the boxes, ranging from 3% to 100%, was controlled by salt solutions (Table 2) [9]. Depending on their initial water saturation and on the RH storage conditions, the cement paste samples gained or lost water. The samples were

* Corresponding author.
E-mail address: sylvie.lorente@insa-toulouse.fr (S. Lorente).

0958-9465/$ - see front matter © 2012 Elsevier Ltd. All rights reserved.
http://dx.doi.org/10.1016/j.cemconcomp.2012.12.009

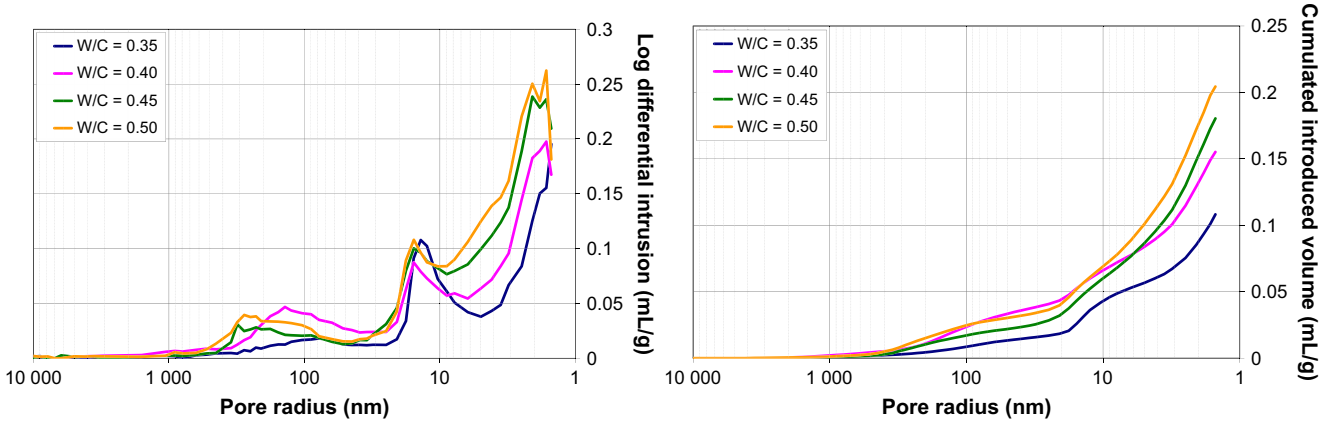

Fig. 1. Mercury intrusion porosimetry on the different CEM V pastes.

Table 1
Water porosity.

W/C ratio	Water porosity (%)
0.35	34.7
0.40	37.8
0.45	39.8
0.50	42.3

Table 2
Salts and their associated relative humidity [9].

Relative humidity (%)	Salt name	Chemical symbol
03	Silica gel	SiO_2
11	Lithium chloride	LiCl
23	Potassium acetate	CH_3COOK
33	Magnesium chloride	$MgCl_2$
43	Potassium carbonate	K_2CO_3
54	Magnesium nitrate	$Mg(NO_3)_2$
70	Potassium iodide	KI
75	Sodium chloride	NaCl
85	Potassium chloride	KCl
95	Potassium nitrate	KNO_3
97	Potassium sulfate	K_2SO_4
100	Ultra-pure water	H_2O

assumed to be in equilibrium with the controlled RH of the sealed box when their monthly mass variation became lower than 0.1%.

Once equilibrium was reached, the hydrogen diffusion coefficient of the sample could be measured. The experimental set-up used in this work is described into details in Ref. [1]. Fig. 2 gives an overview of it. The diffusion tests were run at the same temperature as the samples equilibrium temperature: 20 °C. A CEM V cement paste sample is sandwiched between a hydrogen and a nitrogen cell. These cells are linked to vacuum pumps to remove the ambient air, which allows the nitrogen and hydrogen gas distribution networks to fill the cells. The gas concentration in the nitrogen cell is measured with a Gas Chromatograph (Varian 450 GC®). Before measuring the concentration of diffused hydrogen in the nitrogen cell, the total gas pressure difference between these two cells has to be canceled in order to be sure that the concentration difference between the two cells is the unique driving force.

The effective diffusion coefficient is calculated from the Fick's law of diffusion [10]. Because we measure the hydrogen flux through the two parallel faces of the samples, we can consider a one-dimensional transfer. Fick's law is given by:

$$J = -D\frac{\partial c}{\partial x} \tag{1}$$

where J is the molar diffusive gas flux (mol s^{-1} m^{-2}), D is the gas diffusion coefficient (m^2 s^{-1}), c is the concentration of hydrogen (mol m^{-3}), and x is the coordinate in the thickness direction (m).

In practice, the hydrogen concentration is maintained constant at c_0 in the hydrogen compartment during the test thanks to a hydrogen pressure sensor. By the same token, the boundary conditions are maintained constant in the opposite compartment.

The amount of hydrogen Q reaching the downstream cell is recorded in time which allows calculating the hydrogen flux. Steady state is reached when the flux becomes constant. Because the boundary conditions are maintained constant on both sides of the sample, the concentration gradient $\partial c/\partial x$ from Eq. (1) is simply calculated as c_0/L, where L is the sample thickness. By plotting directly the term QL/Sc_0 as a function of time, where S is the sample cross section, we obtain a curve which becomes a straight line in steady state, and which slope is the diffusion coefficient.

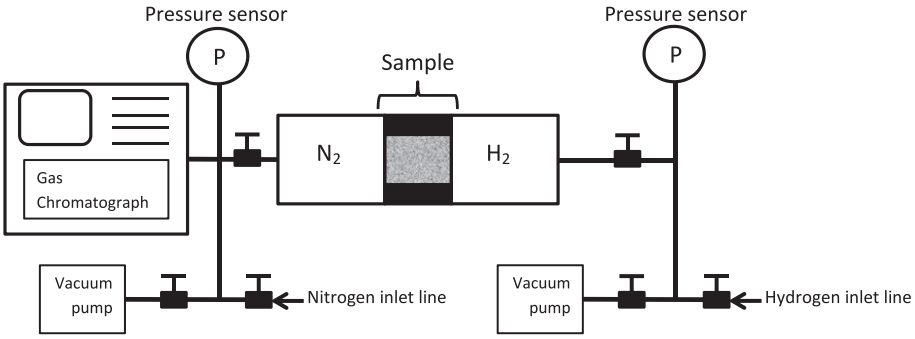

Fig. 2. Hydrogen diffusion experimental set-up.

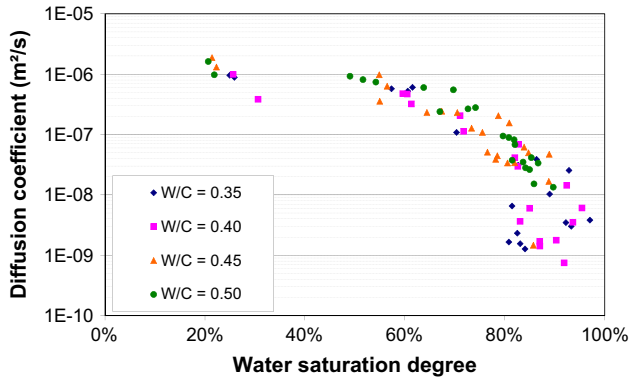

Fig. 3. Experimental hydrogen diffusion coefficient as a function of the water saturation degree.

We used scale analysis [11] to help us estimate the time needed to reach steady state in order to optimize the duration of the experiments. Indeed, considering that the orders of magnitude of the hydrogen concentration c and thickness x are respectively Δc the concentration difference between the two faces of the sample, and L the material thickness, the continuity equation, also known as Fick's second law of diffusion in this case, can be written as

$$\frac{\partial c}{\partial t} = D\frac{\partial^2 c}{\partial x^2} \Rightarrow \frac{\Delta c}{t_{ss}} D \frac{\Delta c}{L^2} \tag{2}$$

$$t_{ss} D \sim L^2 \tag{3}$$

which means that the time to steady state, t_{ss}, multiplied by the diffusion coefficient should remain constant.

Once the diffusion coefficient is obtained, the water saturation degree is measured through water porosity tests following the protocol proposed in Ref. [12].

We present in Fig. 3 the experimental hydrogen diffusion coefficient as a function of the water saturation level. Whatever the value of the W/C ratio, the water saturation level has little impact on the hydrogen diffusion coefficient until the water saturation level is 0.6, which indicates that direct paths exist for the hydrogen transfer through connected pores. From a water saturation level between 60% and 80%, the hydrogen diffusivity loses about two orders of magnitude in a regular fashion. The decreasing slope does not seem to be dependent on the W/C ratio. Next, when the water saturation level is about 85% the hydrogen diffusion coefficient continues to decrease regularly for the highest W/C ratios. This is not the case for W/C = 0.4 and W/C = 0.35 for which the diffusion coefficient exhibits a strong discrepancy of almost two orders of magnitude. For such materials, the relative volumetric proportion of large size pores is smaller than for materials with higher W/C ratios. As a consequence, the hydrogen transfer is controlled by the saturation of the smallest pores which are randomly connected to the biggest pores. According to Ref. [1] results on hydrogen diffusion could be used to describe the diffusion of other gas provided not only the pore network is the same but also the size of the other gas molecule is similar; this is for example the case for nitrogen or helium.

3. Modeling of hydrogen diffusion

Mohycan (MOdèle pour la diffusion d'HYdrogène à travers des CANaux), the model developed in our research group, calculates the hydrogen diffusion coefficient through a virtual pore network as a function of the saturation degree [14]. For the sake of clarity, we present here the philosophy with which the model *Mohycan* was built.

When the mean free path of gas molecules is of the same order of magnitude as the pore radius, collisions with the pore walls are more frequent than between molecules, and free molecule diffusion, named also Knudsen diffusion, prevails. When the pore radius is large enough, molecular diffusion is the main mechanism.

For a dry porous material, the Knudsen number is given by:

$$Kn = \frac{\lambda}{2r} \tag{4}$$

We define D_c as the equivalent diffusion coefficient through one pore channel, D_M as the diffusivity in the molecular diffusion mode, and D_K as the diffusion coefficient in the Knudsen diffusion mode. When the Knudsen number is greater than 10, Knudsen diffusion is the main mechanism and $D_c = D_K$. If the Knudsen number is lower than 0.1, molecular diffusion prevails and $D_c = D_M$. Between these two diffusion values, the two mechanisms are of the same order magnitude. This is the range of variation of the Knudsen number in the case of cement-based materials due to the large heterogeneity of their pore size [4].

The equivalent molecule free path, λ_e, is given by [15]:

$$\frac{1}{\lambda_e} = \frac{1}{\lambda} + \frac{1}{r} \tag{5}$$

where r is the pore radius, and λ is the molecule mean free path.

According to [16], we have:

$$D_K = \frac{2r}{3}\bar{v} \tag{6}$$

$$D_M = \frac{3\pi}{16}\bar{v}\lambda_e \tag{7}$$

$$\bar{v} = \sqrt{\frac{8RT}{\pi M}} \tag{8}$$

where M the molar mass, and $\bar{v}$ is the mean thermal molecular velocity.

From Eq. (5), and according to [17], the following equation can be written:

$$\frac{1}{D_c} = \frac{1}{D_M} + \frac{1}{D_K} \tag{9}$$

The various levels of water saturation in the pores are simulated by depositing layers of water molecules. The thickness of the water layer is assumed to be constant along the pores. In an ideal pore with round cross section, the space available for gas transport is:

$$r_g = r - \delta \tag{10}$$

where r_g is the gas space radius, r is the radius of the considered pore, and δ is the water layer thickness, calculated as the layers number times the water molecule diameter.

If $\delta \geqslant r$, the pore is fully saturated with water. In a pore with a non-constant section, and a total length of L_{pore}, the portion of length where $\delta \geqslant r$ is noted ξ (Fig. 4).

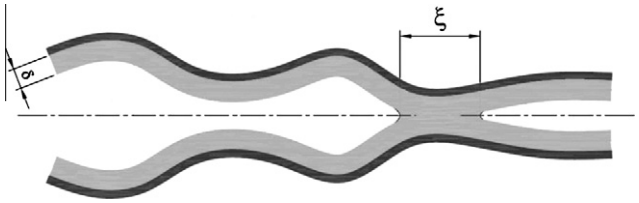

Fig. 4. Water layer (δ) and water obstacle (ξ) in a pore [13].

D_c, the diffusion coefficient through the pore channel accounts for the diffusion through the two media gas and liquid.

$$\frac{L}{D_c} = (L_{pore} - \xi)\left(\frac{1}{D_M} + \frac{1}{D_K}\right) + \frac{\xi}{D_l} \tag{11}$$

where D_l is the diffusion coefficient through liquid phase ($D_l = 10^{-9}\ m^2\ s^{-1}$ [13]).

Mohycan creates a virtual pore network from mercury intrusion porosimetry data which are discretized into pore families. Each pore family has a variable round cross section, the radius of which is a linear function of the channel length (Fig. 5). To differentiate in the model each of the pore families, the subscript i is used.

When the material is partially saturated, the ξ_i length is calculated as

$$\xi_i = \int_0^{L_{pore,i}} (r < \delta_i)dx = (\delta_i > r_{min,i}) \int_{r_{min,i}}^{\delta_i} \bar{\bar{J}}(r)dr \tag{12}$$

where the logical expression $(r < \delta_i)$ means that the factor () equals 1 if true, and 0 if false, and $\bar{\bar{J}}(r)$ is the Jacobian matrix. $r_{min,i}$ and $r_{max,i}$ are respectively the smallest and the biggest pore radius of the family i.

At any pore radius r, the local diffusion coefficient is

$$D_{c,i} = (r > \delta_i)\left[\frac{1}{D_{K,i}(r-\delta_i)} + \frac{1}{D_{M,i}(r-\delta_i)}\right]^{-1} + (r \leqslant \delta_i)D_l \tag{13}$$

while the average value of the gas diffusion coefficient along the pore channel of length $L_{pore,i}$ is given by:

$$\frac{1}{\overline{\overline{D}}_{c,i}} = \frac{1}{\bar{v}L_{pore,i}} \int_{\delta_i}^{r_{max,i}} \frac{a(r-\delta_i)+b}{r-\delta_i} \bar{\bar{J}}(r)dr + \frac{1}{L_{pore,i}D_l}\xi_i \tag{14}$$

where

$$a = \frac{16}{3\pi\lambda_e} \tag{15}$$

$$b = \frac{3}{2} + \frac{16}{3\pi} \tag{16}$$

Next, we move from the diffusion coefficient expressed with Eq. (14), at the scale of the pore channel to D_e, the effective diffusion coefficient, at the scale of the material, by invoking the definition of the material porosity.

$$\phi = \frac{\sum_i N_i A_{c,i} L_{pore,i}}{A L_{material}} = \sum_i \phi_i \tag{17}$$

where N_i is the number of pore in family i, $A_{c,i}$ is the cross section ($A_{c,i} = \pi r_i^2$), $L_{material}$ is the material thickness, A the material cross section, and ϕ_i is the local porosity attributed to the pores of radius r_i.

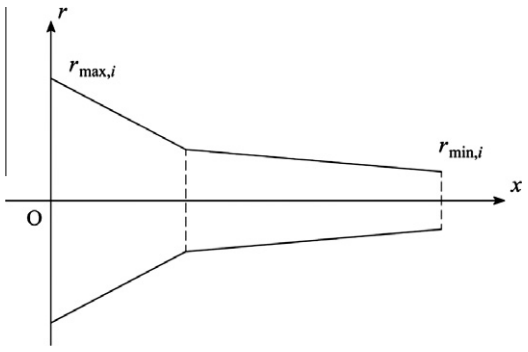

Fig. 5. Example of a pore family [13].

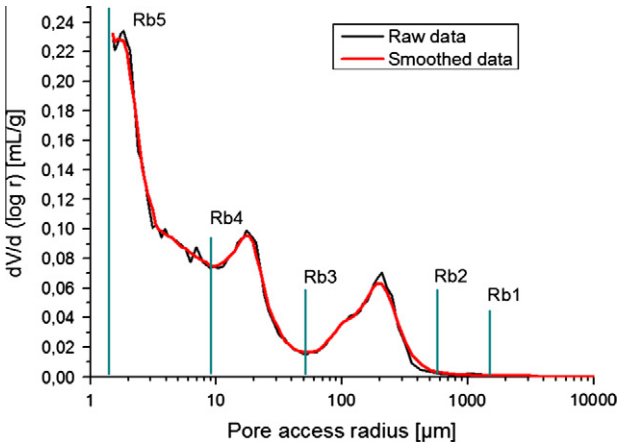

Fig. 6. Pore size distribution obtained with mercury intrusion porosimetry (smoothed data). Results obtained on CEM V cement paste with W/C = 0.45.

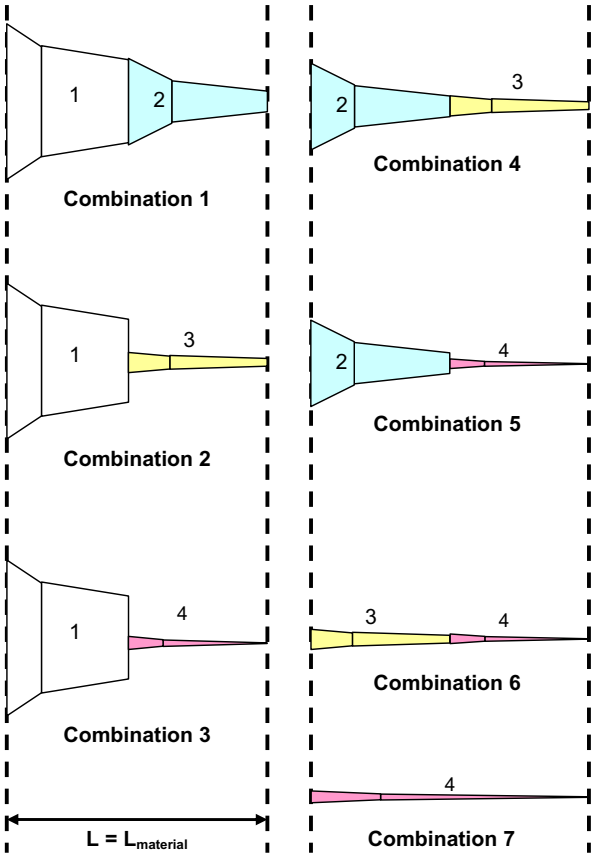

Fig. 7. Pore family combinations.

Calling $f_{g,i}$, the volumetric gas fraction of one given pore family i, $V_{g,i}/V_g$, the effective diffusion coefficient reads [14]

$$D_e = (1 - S_l)\phi \sum_i \overline{D}_{c,i} N_i f_{g,i} \tag{18}$$

where S_l is the water saturation degree.

The virtual pore network needed to run *Mohycan* is obtained by discretizing into 4 pore families the pore network distribution obtained from mercury intrusion porometry data, an example of which is provided in Fig. 6. The five boundaries of the 4 pore families are chosen as follows:

Table 3
Different cases of pore arrangements.

Cases	A (%)	B (%)	C (%)	D (%)	E (%)	F (%)	G (%)
P_1	0	0	10	25	50	75	100
P_2	0	10	10	25	50	25	0
P_4	0	10	10	25	50	100	100

- The first boundary is the largest pore radius for which $\frac{dV}{d(\log r)} > 0$.
- The second boundary is located at the abscissa where $\frac{dV}{d(\log r)} = 5\%$ of the curve peak maximum.
- The third and fourth boundaries are placed on the local minimum between two peaks, i.e. where $\frac{d\left(\frac{dV}{d(\log r)}\right)}{dr} = 0$.
- The last boundary is the smallest pore radius investigated with mercury porometry (=1.5 nm).

We documented in previous work [13,18], the influence of the boundaries radii and virtual network tortuosity on the CEM I cement pastes gas diffusion. Today the model can combine two by two any kind of pore family detected by mercury intrusion porometry. The only constraint in the assembling of the pore families is the one due to the very principle of measurement of mercury porometry, namely the fact that the biggest pores are filled by mercury before the smallest pores. This leads to 6 ways of combining the pore families to which we add another pore family constituted only by the family of the smallest pores (see Fig. 7) due to the high volume of this type of pores. The model user can choose the proportions of combinations 1, 2 and 4 (P_1, P_2, P_4) in the construction of the virtual pore network (see Fig. 7) and can therefore study the impact of the pore arrangement. In our study, 7 cases are investigated. They are described in Table 3. Calling N_{ij} the number of pores resulting of the combination of the pore family i and the pore family j, we obtain: $N_{12} = P_1N_1$, $N_{13} = P_2N_1$, $N_{14} = (1 - P_1 - P_2)N_1$, $N_{23} = P_4\ N_2 - P_1P_4\ N_1$, $N_{24} = (N_2 - N_1P_1)(1 - P_4)$, $N_{34} = N_3 - P_4\ N_{2+} N_1(P_4P_1 - P_2)$, $N_{44} = N_4 - N_3 + N_2(2P_4 - 1) - N_1(1 - 2P_1 - 2P_2 + 2P_1 P_4)$.

4. Results

The input data necessary to create the virtual pore network are the total pore volume and the access pore diameter to mercury intrusion. Although, other investigation techniques exist, the ones used in this work are both simple and accurate enough to obtain a pore network that corresponds to the mercury porosimetry pore size distribution. Because in mercury intrusion porometry the biggest pores are filled by mercury before the smallest pores, the assembling of two pore families always fulfills this requirement. The results are shown in Fig. 8.

4.1. Influence of the gas pore access

Presented in Fig. 9, is the evolution of the diffusion coefficient as a function of the water saturation level for various values of the gas pore access τ^*, for a combination of pores corresponding to case D. Case D was chosen because it presents the most equilibrated pore families distribution between the seven combinations, in terms of pore families number. The gas pore access is calculated as the ratio between the connected pores path length and the material thickness. The effective diffusion coefficient is given by:

$$D_e = \frac{1}{\tau^*}(1 - S_l)\phi\sum_i \overline{D}_{c,i}N_i f_{g,i} \tag{19}$$

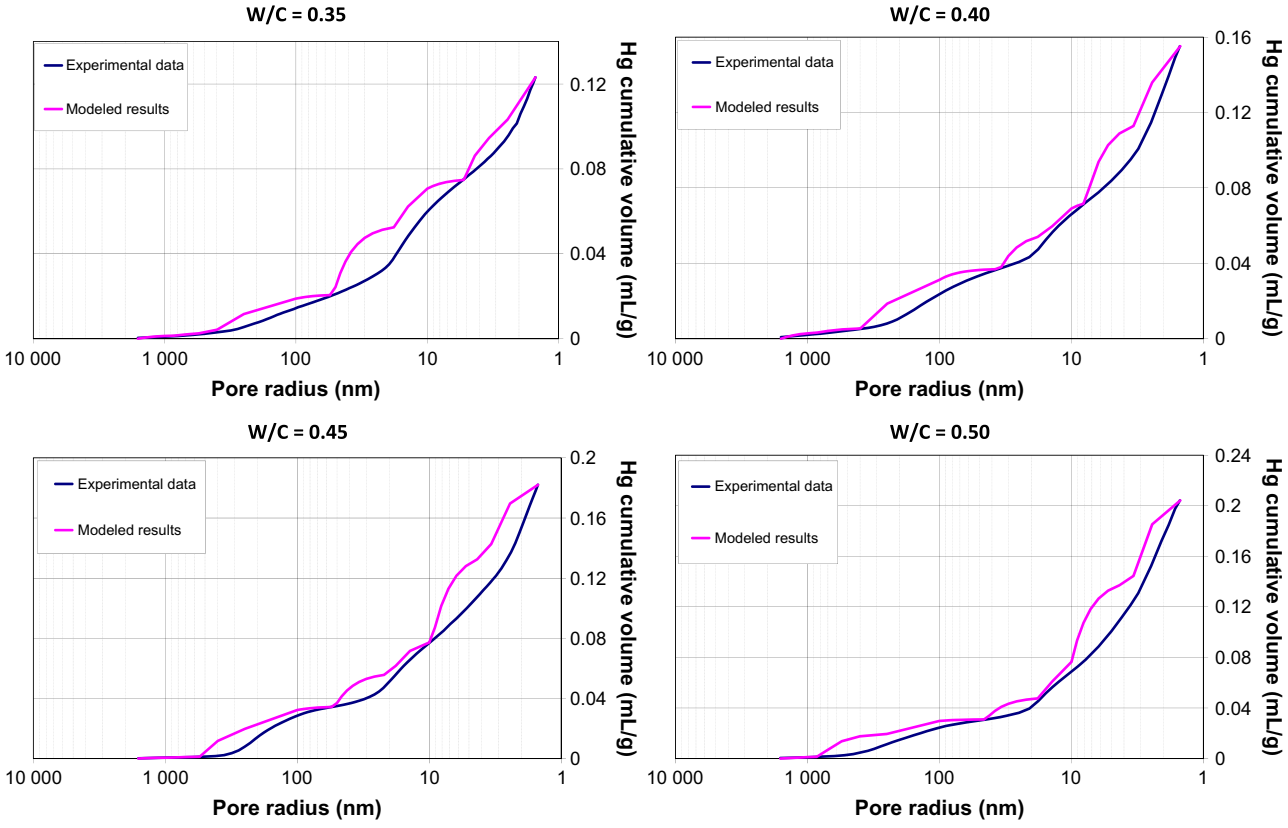

Fig. 8. Modeled and experimental pore size distributions.

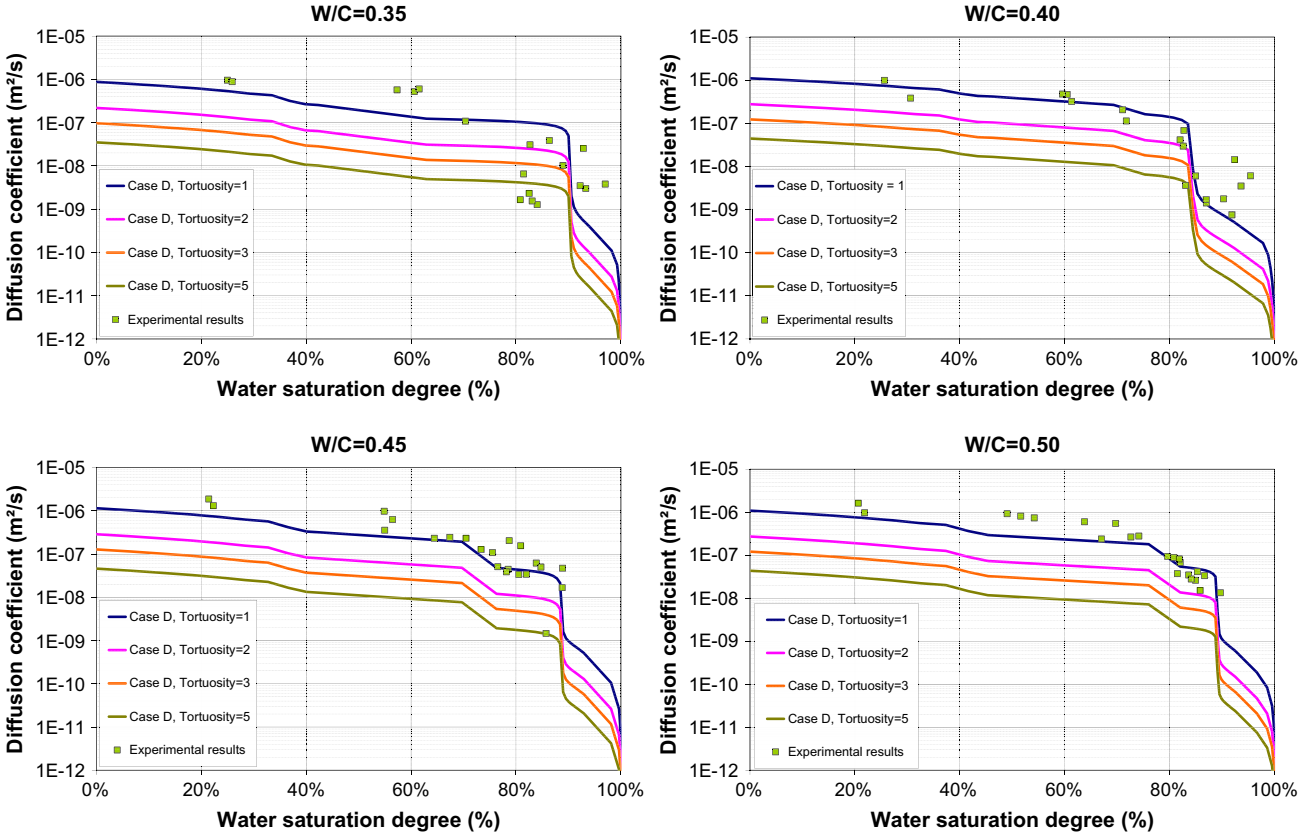

Fig. 9. Modeled diffusion coefficients for various gas pore network access τ^*.

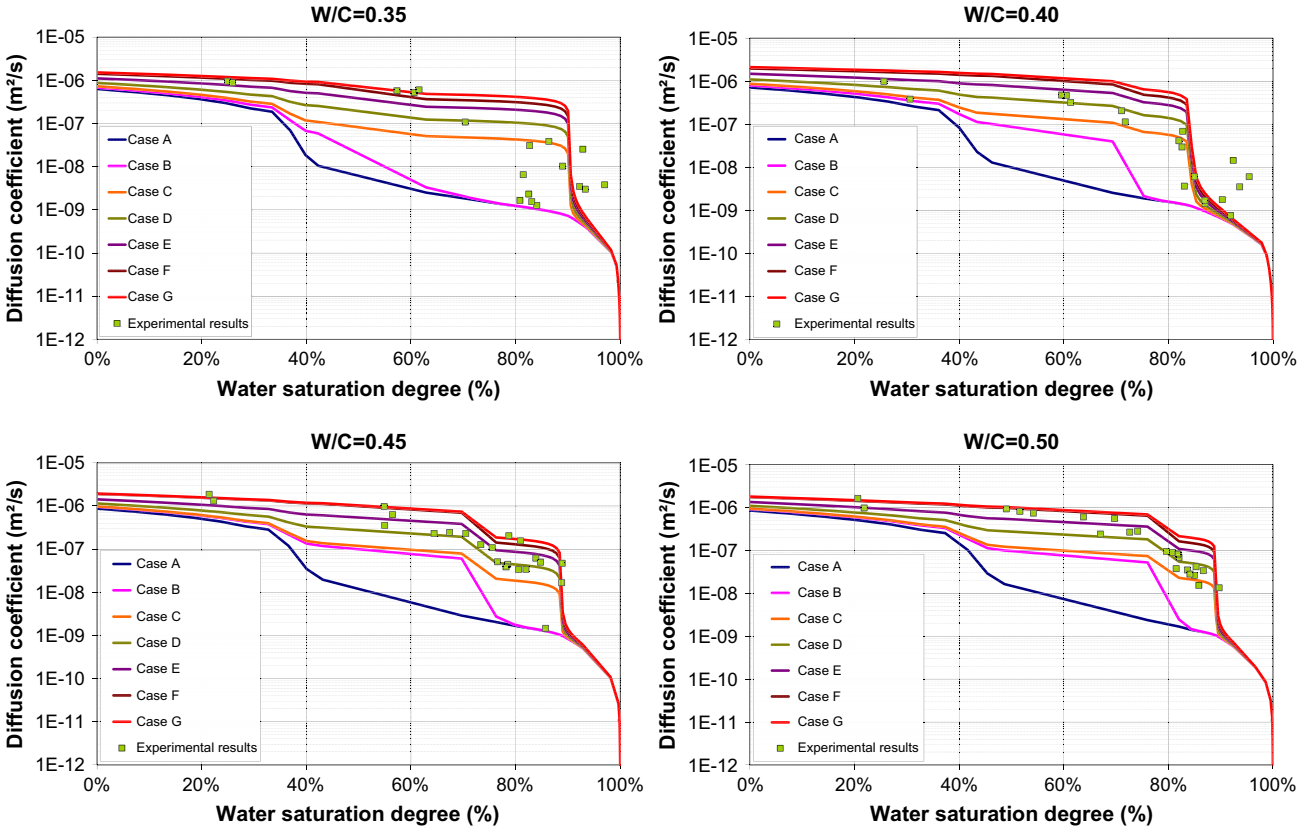

Fig. 10. Impact of the pore distribution on the modeled diffusion coefficients.

The tortuosity, as it was defined in the literature [4,19], is a unique macroscopic parameter defining the geometry of the pore network at the scale of the material. Here, the gas pore access τ^*, is also a geometrical macroscopic parameter. Yet it varies with the saturation level of the material.

As long as the saturation level remains lower than 80%, the best curve fitting is the one corresponding to $\tau^* = 1$, which means that the gas path is direct through the connected pores. This trend persists for the two highest water-to-cement ratios. For W/C = 0.35 or 0.40 the dispersion in the value of the experimental diffusion coefficient is such when the water saturation level is greater than 80% that it becomes extremely difficult to derive any conclusion.

4.2. Influence of virtual pore network distribution

In this section, we maintained $\tau^* = 1$ and checked the impact of the pore families combinations on the prediction of the hydrogen diffusion coefficient for each value of the water saturation level and the water-to-cement ratio. Moving from case A to G means that the relative proportion of pores of bigger size increases. Fig. 10 shows the evolution of the diffusion coefficient as a function of the water saturation level for the different cases tested. Whatever the W/C ratio, a pore network constituted with only the smallest pore sizes (case A) does not represent the reality of the material. We see from Fig. 10 that increasing the proportion of bigger pores leads to predicting diffusion coefficients which values are closer to the measured values. When W/C = 0.35, the pore combinations chosen do not capture the experimental diffusion coefficients all over the range of water saturation. If cases F or G, with the higher proportion of big pores, provide numerical diffusion coefficients close to the measured value when $S_l < 60\%$, cases C or D with a more homogeneous distribution of pore sizes seem to correspond better to the experimental data. Yet, again, the discrepancy in the experiments results makes it difficult to derive definitive conclusions. The same is true when W/C = 0.40 although case D seems to catch the drastic drop in the diffusion coefficient when the water saturation level is about 85%. For W/C = 0.45 and 0.50, we see that case E, in which a homogeneous distribution of pores is preferred, seems to correspond at best to the actual pore network arrangement. That virtual pore network allows indeed predicting hydrogen diffusion coefficients in good agreement with the experimental results.

5. Conclusion

This paper focused on the diffusion of hydrogen through hardened cement pastes with mineral additions (CEM V cement). The experimental results consisted in the evolution of the diffusion coefficient with the water saturation level of cement pastes with different water-to-cement ratios.

By creating a virtual pore network, we proposed a description of the pores arrangement in agreement with results obtained from mercury porosimetry. The virtual pore network serves as basis for the calculation of a theoretical hydrogen diffusion coefficient that accounts for the different types of gas transfer depending on the pores size, and for the gas diffusion through water when the material is partially saturated. The impact of the material saturation was investigated both experimentally and numerically, proving the strong impact of the water saturation level on the diffusion coefficient when $S_l > 80\%$. It was shown that the water saturation level has little impact on the hydrogen diffusion coefficient until the water saturation level is 0.6, which indicates that direct paths exist for the hydrogen transfer through connected pores. A systematic study of the pore arrangements impact on the diffusion coefficient allowed approaching the actual pore connections. The hydrogen transfer is controlled by the saturation of the smallest pores which are randomly connected to the biggest pores.

References

[1] Sercombe J, Vidal R, Gallé C, Adenot F. Experimental study of gas diffusion in cement paste. Cem Concr Res 2007;37(4):579–88.
[2] Frizon E, Gallé C. Experimental investigations of diffusive and convective transport of inert gas through cement pastes. J Porous Media 2009;12(3):221–37.
[3] Ohama Y, Demura K, Kobayashi K, Satoh Y, Morikawa M. Pore-size distribution and oxygen diffusion resistance of polymer-modified mortars. Cem Concr Res 1991;21(2–3):309–15.
[4] Houst YF, Wittmann FH. Influence of porosity and water-content on the diffusivity of Co_2 and O_2 through hydrated cement paste. Cem Concr Res 1994;24(6):1165–76.
[5] Klink T, Gaber K, Schlattner E, Setzer MJ. Characterisation of the gas transport properties of porous materials by determining the radon diffusion coefficient. Mater Struct 1999;32(224):749–54.
[6] Sharif A, Loughlin KF, Azad AK, Navaz CM. Determination of the effective chloride diffusion coefficient in concrete via a gas diffusion technique. ACI Mater J 1997;94(3):227–33.
[7] AFNOR. NF EN 197-1. Composition, spécifications et critères de conformité des ciments courants: AFNOR; 2001.
[8] Ramachandra VS, Beaudoin JJ. Handbook of analytical techniques in concrete science and technology. Principles, techniques and applications. 2001 ed. William Andrew publishing; 2001.
[9] Greenspan L. Humidity fixed-points of binary saturated aqueous-solutions. J Res Nat Bur Stand Section A – Phys Chem 1977;81(1):89–96.
[10] Fick A. Concerns diffusion and concentration gradient. J Membrane Sci 1995;100:33–8.
[11] Bejan A, Lorente S. Appendix. Design with Constructal Theory. John Wiley & Sons, Inc.; 2008. p. 491–517.
[12] AFNOR. NF EN 1936. Détermination des masses volumiques réelle et apparente et des porosités ouverte et totale: AFNOR; 2007.
[13] Cussler EL. Diffusion. Mass transfer in fluid systems. Cambridge: Cambridge University Press; 1997.
[14] Vu TH, Frizon F, Lorente S. Architecture for gas transport through cementitious materials. J Phys D – Appl Phys 2009;42(10):9.
[15] Schüth F, Sing KSW, Weitkamp J. Handbook of porous solids. Wiley; 2002.
[16] Aryanpour G, Abbasi MH. Computer simulation of ordinary gas transfer in tubes. J Porous Media 2005;8(4):379–91.
[17] Scott DS, Dullien FAL. Diffusion of ideal gases in capillaries and porous solids. AIChE J 1962;8(1):113–7.
[18] Vu TH. Caractérisation de la phase solide et transferts de gaz dans les milieux poreux insaturés. Etude expérimentale et modélisation appliquées à la diffusion de l'hydrogène dans les matériaux cimentaires. Université de Toulouse, Toulouse; 2009.
[19] Bejan A, Dincer I, Lorente S, Miguel AF. A.H.R. porous and complex flow structures in modern technologies. New York: Springer Verlag; 2004.